Robust pedestal-free pulse compression in cubic-quintic nonlinear media

K. Senthilnathan,[1] Qian Li,[1] K. Nakkeeran,[2] and P. K. A. Wai[1]
[1]*Photonics Research Center and Department of Electronic and Information Engineering, The Hong Kong Polytechnic University, Hung Hom, Kowloon, Hong Kong, China*
[2]*School of Engineering, Fraser Noble Building, King's College, University of Aberdeen, Aberdeen AB24 3UE, Scotland, United Kingdom*
(Received 18 June 2008; revised manuscript received 13 August 2008; published 24 September 2008)

We consider the evolution of nonlinear optical pulses in cubic-quintic nonlinear media wherein the pulse propagation is governed by the generalized nonlinear Schrödinger equation with exponentially varying dispersion, cubic, and quintic nonlinearities and gain and/or loss. Using a self-similar analysis, we find the chirped bright soliton solutions in the anomalous and normal dispersion regimes. From a stability analysis, we show that the soliton in the anomalous dispersion regime is stable, whereas the soliton in the normal dispersion regime is unstable. Numerical simulation results show that competing cubic-quintic nonlinearities stabilize the chirped soliton pulse propagation against perturbations in the initial soliton pulse parameters. We characterize the quality of the compressed pulse by determining the pedestal energy generated and compression factor when the initial pulse is perturbed from the soliton solutions. Finally, we study the possibility of rapid compression of Townes solitons by the collapse phenomenon and the exponentially decreasing dispersion. We find that the collapse could be postponed if the dispersion increases exponentially.

DOI: 10.1103/PhysRevA.78.033835 PACS number(s): 42.81.Dp, 42.65.Tg, 05.45.Yv

I. INTRODUCTION

The generation of ultrashort optical pulses has received much attention owing to their wide applications in many different areas such as ultrahigh-bit-rate optical communication systems, ultrafast physical processes, infrared time-resolved spectroscopy, optical sampling systems, etc. [1–3]. In general, it is difficult to produce very short optical pulses even from the best available laser sources. Therefore optical pulse compression techniques have been utilized to generate optical pulses shorter than those produced by lasers or amplifiers. Optical pulse compression can be classified into two different types. The first is linear compression of chirped pulses using a dispersive fiber delay line or grating pairs. The second is nonlinear compression based on the interplay between self-phase modulation and group velocity dispersion using either a soliton or adiabatic effect [3]. In soliton effect compression, the compressed pulse typically is a sharp, narrow spike centered on a broad low-intensity pedestal which contains a large proportion of the pulse energy. In optical communication systems, a broad pedestal is undesirable because it will overlap with adjacent pulses and results in intersymbol interference. A number of pedestal suppression techniques have been proposed to block the low-intensity tails of the compressed pulses [4]. Much of the energy of the initial pulse, however, is also discarded in the process. Adiabatic pulse compression, in principle, can achieve pedestal-free compression, but it is difficult to maintain the adiabatic condition throughout the compression process.

Contrary to the above-discussed conventional pulse compression techniques, a technique has been proposed based on filamentation and plasma generation in the high-intensity region [5]. When the intensity of the incident field is high enough in the range of 10^{13}–10^{14} W/cm^2 or the intensity reaches the value where the Kerr nonlinearity saturates, important physical effects like self-focusing, plasma defocusing, etc., come into play. When a pulse with power exceeding the critical power for self-focusing, P_{cr}, propagates in gases it supports a narrow coherent structure known as filaments. The filament is generated after the dynamical balance of two counteracting physical effects: namely, focusing due to the Kerr effect and defocusing due to plasma generated by multiphoton ionization. The filament has been observed in gases as air [6], in solids as silica glasses [7], and in liquids [8].

Recently, much interest has been focused on the compression of linearly chirped pulses. Moores suggested that chirped solitary pulses can be compressed more efficiently if the dispersion decreases approximately exponentially [9]. A self-similar analysis has been utilized to study linearly chirped pulses in optical fibers and fiber amplifiers. The self-similar analysis for the nonlinear Schrödinger (NLS) equation with constant gain has revealed that the interplay of normal dispersion, nonlinearity, and gain produces a linearly chirped pulse with a parabolic intensity profile which resists the deleterious effects of optical wave breaking [10]. The generation of bright and dark self-similar solitary pulses has been investigated using a NLS-type equation in the presence of gain [11]. Chirped solitary pulse compression has been demonstrated in these optical amplifiers. Using the self-similar analysis, we have shown that chirped Bragg solitary pulses can be generated near the photonic band gap of nonuniform-fiber Bragg gratings. We have also investigated pedestal-free Bragg soliton pulse compression [12]. Using the Hirota bilinear method and variational analysis, we have shown that the intensity and the chirp of the chirped soliton for an exponentially decreasing dispersive medium increase exponentially, while its width decreases exponentially. These properties are consistent with self-similar behavior [13].

When an optical pulse is compressed, its peak intensity increases, while the pulse width decreases. When the pulse peak intensity is sufficiently large, the field-induced change of the refractive index is no longer described by the usual Kerr-type nonlinearity—i.e., $n(\omega,I)=n_0(\omega)+n_2I$, where $n(\omega,I)$ is the refractive index of the medium, $n_0(\omega)$ is the refractive index of the medium for weak input optical power,

ω is the angular frequency, n_2 is the Kerr constant, and I is the intensity of the optical pulse. A higher-order nonlinear effect such as the quintic nonlinearity will have to be taken into account and the refractive index will have to be modified to be $n(\omega,I)=n_0(\omega)+n_2I-n_4I^2$, where n_4 is the quintic nonlinearity coefficient. The coefficients n_2 and n_4 are related to the third-order $\chi^{(3)}$ and fifth-order $\chi^{(5)}$ susceptibilities through $n_2=3\chi^{(3)}/(8n_0)$ and $n_4=-5\chi^{(5)}/(32n_0)$. Pulse propagation in the presence of competing cubic-quintic nonlinearities has received much attention lately because competition between nonlinearities of different orders could lead to strong stabilization of pulse propagation [14]. Higher-order nonlinearities must be considered if the optical pulse intensity is high or the nonlinear coefficients of the materials are large—for instance, in semiconductor doped glasses [14,15]. One example of the effect of competing nonlinearities is the stabilization of vortices and vortex tori in cubic-quintic nonlinear media [16–19]. In the constant-dispersion case, the bright and dark solitons have been extensively investigated in the cubic-quintic nonlinear media [20,21]. The bright and dark quasi-solitons for the cubic-quintic nonlinearity have also been studied [22]. In recent years, a number of experiments reported the measurement of the cubic-quintic nonlinearity [23]. More recently, we have investigated the existence of chirped bright solitons in cubic-quintic nonlinear media with exponentially decreasing dispersion [24]. In this paper, we investigate pedestal-free pulse compression of the chirped bright soliton pulse under the influence of cubic and quintic nonlinearities. Numerical results reveal that competing cubic and quintic nonlinearities can stabilize the pulse propagation and will lead to more robust pulse compression. As a special case, we also discuss chirped Townes solitons in pure quintic media—i.e., power-law nonlinearity—and study the possibility of rapid pulse compression by wave collapse and exponentially decreasing dispersion. We note that the pure quintic nonlinearity aptly models the Tonks-Girardeau (TG) regime in Bose-Einstein condensation (BEC).

The rest of the paper is organized as follows. Section II discusses the theoretical model and the origin of the fifth-order (quintic) nonlinearity. In Sec. III, we present the chirped bright soliton solutions. We then determine the relations among the dispersion, cubic nonlinear, and quintic nonlinear lengths. Using numerical simulations, we study the effects of the perturbations in the soliton parameters such as the peak power and chirp on the quality of compressed pulses. These numerical results show that the chirped bright soliton in the anomalous dispersion regime is stable, whereas it is unstable in the normal dispersion regime. In Sec. IV, we study the chirped Townes solitons in pure quintic nonlinearity and discuss possible applications to BEC. Finally, we conclude in Sec. V.

II. THEORETICAL MODEL

Cubic-quintic nonlinearity arises from a nonlinear correction to the refractive index of a medium in the form $\delta n=n_2I-n_4I^2$, and the coefficients $n_2, n_4>0$ determine the nonlinear response of the medium. Formally, the expression for δn may be obtained by an expansion of a saturable nonlinearity of the form $\delta n=n_2I[1+(n_4/n_2)I]^{-1}$ under the assumption of self-focusing as $d(\delta n)/dI$. However, the cubic-quintic model changes the sign of focusing at a critical intensity $I_c=n_2/2n_4$. Experimental measurement of the nonlinear dielectric response in para-toluene salfonate (PTS) optical crystal confirmed the observations [14]. Cubic-quintic nonlinearities can also be obtained by doping a fiber with two appropriate semiconductor materials. One should be positive $n_2^{(1)}>0$ and have a large saturation intensity $I_{\text{sat}}^{(1)}$, and the other should be negative $n_2^{(2)}<0$ with nearly the same magnitude and have a low saturation intensity—i.e., $I_{\text{sat}}^{(2)}\ll I_{\text{sat}}^{(1)}$ [20].

Pulse propagation in a medium with cubic-quintic nonlinearities is governed by the generalized cubic-quintic NLS (CQNLS) equation

$$i\frac{\partial A}{\partial z}-\frac{\beta(z)}{2}\frac{\partial^2 A}{\partial \tau^2}+\gamma(z)|A|^2A-\delta(z)|A|^4A-i\frac{g(z)}{2}A=0, \tag{1}$$

where $A(z,\tau)$ is the slowly varying envelope of the axial electrical field, τ is the retarded time, z is the propagating distance, $\beta(z)$ is the group velocity dispersion, and $g(z)$ is the distributed gain or loss function. The cubic and quintic nonlinear parameters are given by $\gamma=2\pi n_2/\lambda_0A_{\text{eff}}$ and $\delta=2\pi n_4/\lambda_0A_{\text{eff}}^2$, where λ_0 is the central wavelength and A_{eff} is the effective core area of the fiber. All physical parameters $\beta(z)$, $\gamma(z)$, $\delta(z)$, and $g(z)$ are functions of the propagation distance z.

We now investigate the chirped soliton solutions of the CQNLS equation by a scaling analysis known as self-similar analysis. We assume the complex function $A(z,\tau)$ in the form

$$A(z,\tau)=Q(z,\tau)\exp[i\Phi(z,\tau)], \tag{2}$$

where Q and Φ are the amplitude and phase of the envelope function A, respectively. In order to study the generation of chirped solitons of Eq. (1), we assume a quadratic phase given by

$$\Phi(z,\tau)=\alpha_1(z)+\frac{\alpha_2(z)}{2}(\tau-\tau_c)^2, \tag{3}$$

where $\alpha_1(z)$ and $\alpha_2(z)$ are functions of z and τ_c is the center of the pulse. By self-similar scaling analysis, we assume that the amplitude depends on the scaling variable θ, which is a combination of variables $\tau-\tau_c$ and some function $\Gamma(z)$ of the variable z. Since the self-similar solutions possess scaling structure, we represent the amplitude $Q(z,\tau)$ as

$$Q(z,\tau)=\frac{1}{\sqrt{\Gamma(z)}}R(\theta)\exp\left[\frac{G(z)}{2}\right]. \tag{4}$$

The scaling variable θ and the function $G(z)$ are given by

$$\theta=\frac{\tau-\tau_c}{\Gamma(z)},\quad G(z)=\int_0^z g(z')dz'. \tag{5}$$

Here $\Gamma(z)$ and $R(\theta)$ are some functions which have to be determined. We also assume that $\Gamma(0)=1$ without loss of generality. Substituting Eqs. (2)–(4) into Eq. (1), the qua-

dratic phase coefficient $\alpha_2(z)$ and the function $\Gamma(z)$ are found to be

$$\alpha_2(z) = \frac{\alpha_{20}}{1 - \alpha_{20} D(z)}, \quad \Gamma(z) = 1 - \alpha_{20} D(z), \tag{6}$$

where $\alpha_{20} = \alpha_2(0) \neq 0$ because the phase is assumed to be a quadratic function of the variable $\tau - \tau_c$ and the cumulative dispersion function $D(z)$ is given by

$$D(z) = \int_0^z \beta(z')dz'. \tag{7}$$

In addition to the above conditions, we also find

$$\frac{d^2R}{d\theta^2} + \frac{2\Gamma^2}{\beta}\frac{d\alpha_1}{dz}R - \frac{2\Gamma\gamma}{\beta}\exp[G(z)]R^3 + \frac{2\delta}{\beta}\exp[2G(z)]R^5 = 0. \tag{8}$$

Note that the coefficients in Eq. (8) are functions of the variable z, but the function $R(\theta)$ depends only on the scaling variable θ. Therefore, Eq. (8) possesses nontrivial solutions $[R(\theta) \neq 0]$ if and only if the coefficients in Eq. (8) are constants, i.e.,

$$-\frac{2\Gamma^2(z)}{\beta(z)}\frac{d\alpha_1}{dz} = \lambda_1, \tag{9}$$

$$\frac{\Gamma(z)\gamma(z)}{\beta(z)}\exp[G(z)] = \lambda_2, \tag{10}$$

$$\frac{\delta(z)}{\beta(z)}\exp[2G(z)] = \lambda_3, \tag{11}$$

where λ_1, λ_2, and λ_3 are constants. Equations (9)–(11) yield

$$\lambda_1 = -\left.\frac{2}{\beta_0}\frac{d\alpha_1}{dz}\right|_{z=0}, \quad \lambda_2 = \frac{\gamma_0}{\beta_0}, \quad \lambda_3 = \frac{\delta_0}{\beta_0}, \tag{12}$$

because $\Gamma(0)=1$ and $G(0)=0$. The parameters $\beta_0 = \beta(0)$, $\gamma_0 = \gamma(0)$, and $\delta_0 = \delta(0)$. Thus for the nontrivial case, Eq. (8) can be written as

$$\frac{d^2R}{d\theta^2} - \lambda_1 R + 2\lambda_2 R^3 + 2\lambda_3 R^5 = 0. \tag{13}$$

The solution of Eq. (9) is

$$\alpha_1(z) = \alpha_{10} - \frac{\lambda_1}{2}\int_0^z \frac{\beta(z')dz'}{[1 - \alpha_{20}D(z')]^2}, \tag{14}$$

where α_{10} is an integration constant. Next we proceed to find the distributed gain function using Eqs. (10) and (11),

$$g(z) = \frac{1}{\eta(z)}\frac{d\eta}{dz} - \frac{\alpha_{20}\beta(z)}{\Gamma(z)}, \tag{15}$$

where we define the function $\eta(z)$ as

$$\eta(z) = \frac{\gamma(z)}{\delta(z)}, \quad \eta(0) = \frac{\gamma_0}{\delta_0}. \tag{16}$$

From Eqs. (10) and (11), the condition for the variation of the quintic nonlinear parameter is

$$\delta(z) = \frac{\gamma^2(z)\Gamma^2(z)}{\beta(z)}\frac{\lambda_3}{\lambda_2^2}. \tag{17}$$

Equations (6), (7), and (12)–(17) are the required conditions for the existence of self-similar solutions in Eqs. (2)–(5) of the generalized CQNLS with distributed coefficients—i.e., Eq. (1). We observed that for the self-similar solutions of Eq. (1), only two of the four parameters $\beta(z)$, $\gamma(z)$, $\delta(z)$, and $g(z)$ in Eq. (1) are free parameters. For example, if $\beta(z)$ and $\gamma(z)$ are chosen to be the free parameters, then $g(z)$ and $\delta(z)$ will be determined from Eqs. (15) and (17) respectively.

Different physical situations lead to different choices of the two free parameters. For example, consider that both the cubic and quintic nonlinear coefficients do not vary with distance; i.e., both $\gamma(z)$ and $\delta(z)$ are constant. A self-similar solution to Eq. (1) exists if the dispersion and gain or loss vary in the form $\beta(z) = \beta_0/(1+\beta_0\alpha_{20}z)^2$ and $g(z) = \beta_0\alpha_{20}/(1+\beta_0\alpha_{20}z)$. If the cubic nonlinear parameter $\gamma(z)$ is constant and there is no gain or loss $[g(z)=0]$, then the dispersion and the quintic nonlinearity must vary exponentially—i.e., $\beta(z) = \beta_0\exp(-\alpha_{20}\beta_0 z)$ and $\delta(z) = \delta_0\exp(-\alpha_{20}\beta_0 z)$. In this case, the function $\Gamma(z) = \exp(-\alpha_{20}\beta_0 z)$. Thus, from Eq. (5), the pulse width will vary exponentially as the dispersion $\beta(z)$. Since we are interested in pedestal-free compression of optical pulses, we will focus on the soliton solutions to CQNLS equation with exponentially varying dispersion in Sec. III. Another special case is pure quintic nonlinearity with no gain or loss—i.e., $\gamma(z) = g(z) = 0$. From Eq. (11), the quintic nonlinearity $\delta(z)$ is then directly proportional to the dispersion $\beta(z)$, which can take any functional form. We will study this special case in Sec. IV.

III. CHIRPED SELF-SIMILAR BRIGHT SOLITONS IN THE ANOMALOUS AND NORMAL DISPERSION REGIMES

In this section, we assume that the cubic nonlinear parameter $\gamma(z)$ is constant and there is no gain or loss—i.e., $g(z) = 0$. The dispersion and quintic nonlinearity therefore vary exponentially as $\beta(z) = \beta_0\exp(-\alpha_{20}\beta_0 z)$ and $\delta(z) = \delta_0\exp(-\alpha_{20}\beta_0 z)$. From Sec. II, the phase and amplitude of the self-similar solutions of the generalized CQNLS equation with distributed coefficients are given by Eqs. (3) and (4). We determine the complex envelope of the bright solitary wave by integrating Eq. (13) and obtain

$$A(z,\tau)=\frac{1}{\tau_0[1-\alpha_{20}D(z)]}\left[\frac{\mp 2\rho_1}{\sqrt{1+\dfrac{8\rho_1^2}{3\rho_2\tau_0^2[1-\alpha_{20}D(z)]^2}}\cosh 2\left[\dfrac{\tau-\tau_c}{\tau_0[1-\alpha_{20}D(z)]}\right]\pm 1}\right]^{1/2}\exp(i\Phi), \tag{18}$$

where $\rho_1(z)=\beta(z)/\gamma(z)$ and $\rho_2(z)=\beta(z)/\delta(z)$. The integration constant λ_1 is chosen to be $1/\tau_0^2$, where τ_0 is the initial pulse width parameter. The upper sign in Eq. (18) corresponds to the soliton in the anomalous dispersion regime, while the lower sign corresponds to that in the normal dispersion regime. In the anomalous dispersion regime, the physical conditions $\beta<0$, $\gamma>0$, and $\delta>0$ (competing cubic-quintic nonlinearities) or $\beta<0$, $\gamma>0$, and $\delta<0$ (cooperating cubic-quintic nonlinearities) should be maintained for the existence of solitons. Similarly, $\beta>0$, $\gamma>0$, and $\delta>0$ (competing cubic-quintic nonlinearities) have to be valid for the soliton in the normal dispersion regime. Equation (18) is a linearly chirped self-similar bright solitary pulse since it propagates in a self-similar manner in a fiber medium under the influence of cubic-quintic nonlinearities. In semiconductor double-doped optical fibers, self-similar solitons in both normal and anomalous dispersion regimes are possible depending on the doping materials, the operating frequency, and the optical pulse intensities [21,24].

A. Length scales

Unlike the conventional soliton in Kerr media, where the dispersion and nonlinear lengths are proportional to each other, we found that the dispersion, cubic, and quintic nonlinear lengths for the self-similar solitons in a cubic-quintic medium follow a harmonic relationship

$$\frac{2\,\mathrm{sgn}(\delta)}{3L_{n_4}(z)}-\frac{\mathrm{sgn}(\gamma)}{L_{n_2}(z)}-\frac{\mathrm{sgn}(\beta)}{L_D(z)}=0, \tag{19}$$

where the dispersion (L_D), cubic (L_{n_2}), and quintic (L_{n_4}) nonlinear lengths are given by

$$L_D(z)=\frac{\tau_0^2\Gamma^2(z)}{|\beta(z)|},\quad L_{n_2}(z)=\frac{1}{|\gamma(z)|P_0(z)},$$

$$L_{n_4}(z)=\frac{1}{|\delta(z)|P_0^2(z)}. \tag{20}$$

Here $P_0=|A_{\max}|^2$ is the peak power of the chirped soliton, where $A_{\max}$ is the maximum amplitude [which is given in Eq. (23)]. Note that all the three length scales vary with distance because the coefficients of the CQNLS equation depend on distance. We note that when the quintic nonlinearity is switched off—i.e., $L_{n_4}\to\infty$—Eq. (19) is reduced to the well-known condition $L_D=L_{n_2}$ for soliton formation in Kerr media. In this case, the linearly chirped bright soliton in Eq. (18) will be reduced to the chirped soliton solution for Kerr nonlinearity [11–13].

From Eq. (18), the energy of the chirped bright soliton is calculated as

$$W=\int_{-\infty}^{\infty}|A|^2d\tau=-\frac{2\rho_1(z)}{\tau_0\Gamma\sqrt{1-b^2}}\ln\frac{1+\sqrt{1-b^2}}{b}\quad(b<1), \tag{21}$$

$$W=\int_{-\infty}^{\infty}|A|^2d\tau=\mp\frac{2\rho_1(z)}{\tau_0\Gamma\sqrt{b^2-1}}\left[\frac{\pi}{2}\mp\sin^{-1}\left(\frac{1}{b}\right)\right]\quad(b>1), \tag{22}$$

where $b=\sqrt{1+8\lambda_3/3\tau_0^2\lambda_2^2}$ is a constant. In terms of length scales, the parameter b can also be written as $b=\sqrt{1+\frac{4L_{n2}(z)}{L_D(z)^2}[\mathrm{sgn}(\beta)\mathrm{sgn}(\gamma)L_D(z)+L_{n2}(z)]}$. Equation (21) represents the energy of the soliton in the anomalous dispersion regime when $b<1$. The upper sign in Eq. (22) corresponds to the soliton energy in the anomalous dispersion regime when $b>1$. The lower sign corresponds to the soliton energy in the normal dispersion regime for all values of $b>0$. The condition $b>1$ (<1) corresponds to $\delta_0/\beta_0>0$ (<0). For optical fibers, the cubic nonlinear coefficient $\gamma>0$. Thus, in the anomalous dispersion regime, the condition $b>1$ means $\delta<0$ representing cooperating cubic-quintic nonlinearities, whereby the effect of dispersion is balanced by the cubic and quintic nonlinearities. The other condition $b<1$ means $\delta>0$ representing the competing cubic-quintic nonlinearities, wherein the effect of cubic nonlinearity is balanced by that of dispersion and quintic nonlinearity. The condition $b=1$ is not of interest because it corresponds to $L_D(z)=L_{n2}(z)$, which is possible only if $L_{n_4}\to\infty$—i.e., $\delta=0$. In the normal dispersion regime, normally $b>1$ because $\mathrm{sgn}(\gamma)>0$. Thus, in the anomalous dispersion regime, the parameter b determines whether the nonlinearities are cooperating or competing.

We find that the soliton solution in the anomalous dispersion regime will approach the chirped soliton solution reported in [11–13] when the coefficient of the quintic nonlinearity approaches zero ($\delta\to 0$). However, the energy of Eq. (22) goes to infinity when $\delta\to 0$ ($\lambda_3\to 0$). Thus, the quintic nonlinearity is crucial to the chirped soliton solutions in the normal dispersion regime. Similarly, the peak intensity and the full width at half maximum (FWHM) are given by

$$A_{\max}^2(z)=P_0=\mp\frac{1}{\tau_0^2\Gamma^2}\frac{2\rho_1(z)}{b\pm 1}, \tag{23}$$

$$\Delta\tau=\tau_0\Gamma(z)\ln[2\pm y+\sqrt{(2\pm y)^2-1}], \tag{24}$$

where $y=1/b$. The upper sign in Eqs. (23) and (24) corresponds to the peak intensity and the pulse width of solitons in the anomalous dispersion regime, while the lower sign corresponds to that in the normal dispersion regime. Note

that Eq. (24) represents the FWHM of the chirped soliton pulse after the compression process. Further, from the same relation, as we know the initial and final widths of the pulse, one can easily determine the pulse compression factor with the relation

$$\frac{\tau_0}{\Delta\tau} = \{\Gamma \ln[2 \pm y + \sqrt{(2 \pm y)^2 - 1}]\}^{-1}. \quad (25)$$

B. Stability of the chirped solitons

Strictly speaking, the localized solution given in Eq. (18) is not a soliton, but rather a solitary wave. It is therefore crucial to determine the stability of the chirped solitons. Ideally, analytical techniques such as the Vakhitov-Kolokolv (VK) criterion should be used to determine the stability of the solitary waves. The VK criterion has been well established for constant-coefficient NLS-type equations (for both cubic and cubic and quintic nonlinearities). However, mathematically the VK criterion is applicable to the ground states of NLS-type equations only. Thus, the VK criterion cannot be applied to analyze the stability of the chirped soliton given in Eq. (18). As a result, we have to resort to using numerical simulations to determine the stability of the chirped solitons. From extensive numerical simulations, we find that the chirped soliton in the anomalous dispersion regime is stable, whereas that in the normal dispersion regime is unstable (for details see Sec. III C). Therefore, hereafter, we focus on pulse compression in the anomalous dispersion regime only.

Before we leave this subsection, we would like to illustrate the relationship between the three length scales discussed in Sec. III A. We consider the case in which the cubic nonlinearity γ=const and gain or loss $g(z)=0$. Thus the dispersion and quintic nonlinearity parameters are given by

$$\beta(z) = \beta_0 \exp(-\sigma z), \quad \delta(z) = \delta_0 \exp(-\sigma z), \quad (26)$$

where $\beta_0 < 0$, $\delta_0 > 0$, and $\sigma = \alpha_{20}\beta_0 > 0$ for dispersion-decreasing fibers. As an example of pulse compression, we consider a semiconductor-doped (chalcogenide AS_2Se_3) fiber of length $L=400$ m. The effective core area of the fiber is assumed to be 10 μm^2. The cubic and quintic nonlinear coefficients are assumed to be $\gamma_0=0.2362$ W^{-1} m^{-1} and $\delta_0 = 0.4724$ W^{-2} m^{-1}, respectively. The initial dispersion β_0 is chosen to be -0.5 ps^2 m^{-1}. The other physical parameters chosen are $\tau_0=5$ ps, $\sigma=0.005$ m^{-1}, $\alpha_{20}=-0.01$ THz^2, and $g=0$. Figure 1 plots the variation of dispersion, cubic, and quintic nonlinear lengths for a soliton solution. From Fig. 1, in the beginning of the compression, the cubic nonlinear length and the dispersion length dominate. As the pulse propagates and compresses, its peak intensity increases and hence the quintic nonlinear length decreases and becomes comparable to the dispersion length and the cubic nonlinear length.

Figure 2 shows the compression of the bright soliton under the influence of the competing cubic-quintic nonlinearities. The compression factor of the above compressor is found to be 7.39. We also numerically integrated Eq. (1) using the exact soliton solution as an initial condition. The numerical results agree very well with the analytical solution as illustrated in Fig. 2.

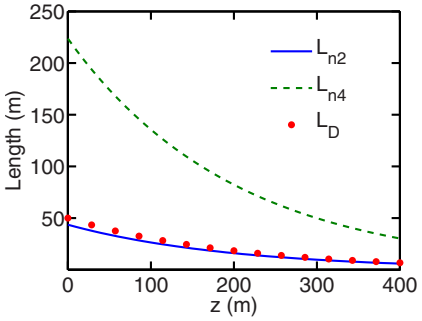

FIG. 1. (Color online) Variation of the dispersion length (dots), cubic nonlinear length (solid line), and quintic nonlinear length (dashed line) for a chirped soliton in a cubic-quintic nonlinear medium. The physical parameters chosen are $\tau_0=5$ ps, $\beta_0=-0.5$ ps^2 m^{-1}, $\sigma=0.005$ m^{-1}, $\gamma_0=0.2362$ W^{-1} m^{-1}, $\delta_0 = 0.4724$ W^{-2} m^{-1}, $\alpha_{20}=-0.01$ THz^2, $g=0$, and $z=400$ m.

C. Perturbations in the initial peak power and chirp

Since Eq. (1) is not integrable, for optical compression applications it is necessary to study the effects of perturbations on the evolution of the solitary-wave solution given in Eq. (18). In the following, we investigate the effect of perturbations in the initial peak power and chirp on the pulse evolution. First, we consider variations in the initial peak power and initial chirp and study the corresponding evolution in peak power and chirp. We determine the quality of the compressed pulse by monitoring the evolution of the pedestal energy generated and the compression factor of the perturbed initial pulse.

Figure 3 shows the deviations in peak power and chirp coefficient at $L=400$ m from the analytic solution when the input peak power deviates from the ideal peak power from -20% to $+20\%$, but the pulse width of the solitary pulse remain unchanged. The choice of fiber and pulse parameters are the same as those in Fig. 1. The dots represent results for competing cubic-quintic nonlinearities ($b<1$), circles represent the results for cooperating cubic-quintic nonlinearities ($b>1$), and crosses represent the results for pure cubic non-

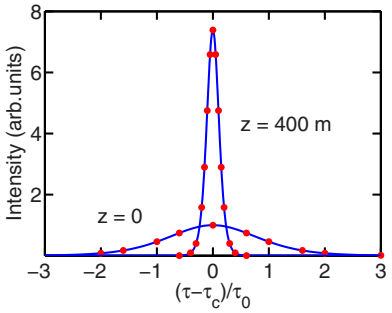

FIG. 2. (Color online) Compression of a chirped bright soliton pulse. The dots and solid lines represent analytical and numerical results, respectively. The parameters chosen are the same as those in Fig. 1.

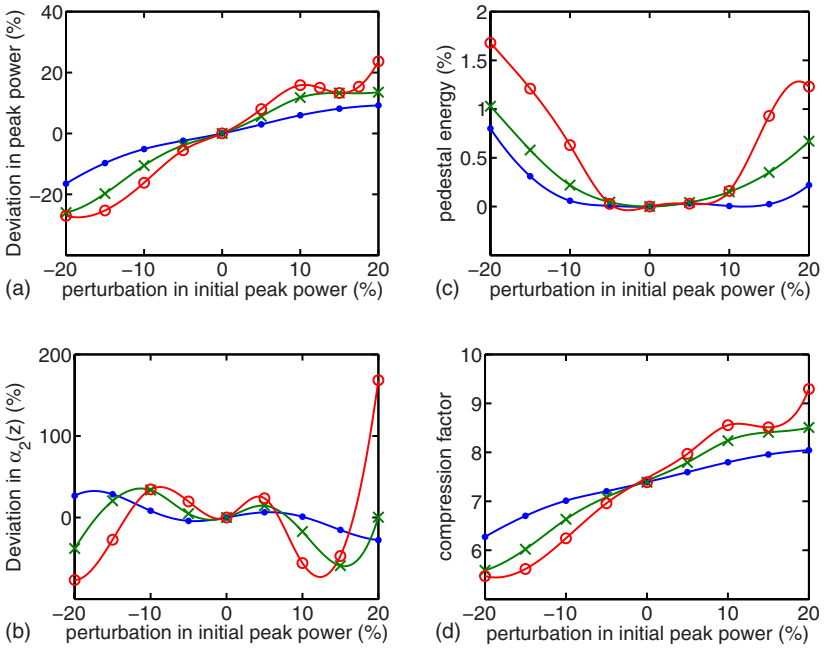

FIG. 3. (Color online) (a) Deviations of the peak power from the exact solution, (b) the chirp coefficient, (c) the pedestal energy, and (d) the compression factor at $L=400$ m when the input peak power deviates from the ideal peak power from −20% to +20%. The physical parameters chosen are the same as those in Fig. 1. The dots represent results for competing cubic-quintic nonlinearities ($\delta_0=0.4724\ \mathrm{W}^{-2}\,\mathrm{m}^{-1}$), circles represent the results for cooperating cubic-quintic nonlinearities ($\delta_0=-0.4724\ \mathrm{W}^{-2}\,\mathrm{m}^{-1}$), and crosses represent the results for pure cubic nonlinearity ($\delta_0=0$).

linearity. Figure 3(a) shows that the deviations of the peak power from the ideal solution is smallest for the case of competing cubic-quintic nonlinearities and largest for cooperating cubic-quintic nonlinearities. Here, it should be emphasized that the larger deviation in the latter case is owing to the beam collapse which occurs in the case of cooperating cubic and quintic nonlinearities. In Fig. 3(a), the deviation in peak power and the perturbation in initial peak power have been calculated with the expression $(P_{\mathrm{perturbed}}-P_{\mathrm{ideal}})/P_{\mathrm{ideal}}\times 100\%$. From Fig. 3(b), the same observation holds for the deviations of the chirp parameter, but the variations in the chirp parameter are more sensitive to the perturbation. Here, the chirp of the perturbed solitary pulse is measured by carrying out a polynomial fit of the phase. From the polynomial fitting, we observe that the chirp remains close to the quadratic chirp since the chirps contributed by all higher-order terms are very small. Based on the numerical results, we observe that the soliton solutions for competing cubic-quintic nonlinearities are more robust to perturbations. The amount of pedestal generated during pulse compression is an important parameter characterizing the quality of the compressed pulses. The pedestal energy is defined as the relative difference between the total energy of the transmitted pulse and the energy of a hyperbolic-secant pulse having the same peak power and width as those of the transmitted pulse—i.e., pedestal energy $(\%)=|E_{\mathrm{perturbed}}-E_{\mathrm{CQ}}|/E_{\mathrm{perturbed}}\times 100\%$. Here, $E_{\mathrm{perturbed}}$ is the energy of the perturbed pulse. Note that the energy of a hyperbolic-secant type pulse (E_{CQ}) in cubic-quintic media is calculated by using curve fitting to obtain the best fit from the data. We use the function $|A|^2=\xi_1/[\xi_2\cosh(2\chi/\xi_3)+1]$ to fit the intensity of the hyperbolic-secant type pulse, where the values of the parameters ξ_1, ξ_2, and ξ_3 are determined by the curve fitting. Figure 3(c) shows the amount of pedestal generated for the corresponding perturbation in peak power. The results show that competing cubic-quintic nonlinearities generate only a small amount of pedestal energy when compared to cooperating cubic-quintic nonlinearities and pure cubic nonlinearity. However, the amount of pedestal generated in all three cases is very small. Even in the worst case in which the initial peak power is only 80% of the ideal value for cooperating cubic-quintic nonlinearities, the pedestal energy is only 1.6%. Figure 3(d) shows the compression factor for the corresponding perturbation in the peak power for all three cases. As expected, the compression factor is the highest for cooperating cubic-quintic nonlinearities and the lowest for the competing case. Thus an optical pulse compressor using competing cubic-quintic nonlinearities are more robust to perturbations of the input pulse parameters at the expense of the compression factor.

Figures 4(a) and 4(b), respectively, show the deviation in peak power and the chirp when the initial chirp of the input pulse deviates from the ideal value. Unlike the perturbations in peak power, the deviation in peak power is small and is very similar in all three cases. The differences in the deviations in chirp value for the three cases are more significant. Again, the deviation of the chirp value is the smallest for competing cubic-quintic nonlinearities and the largest for cooperating case. Figures 4(c) and 4(d) show the pedestal energy and compression factor, respectively, for the corresponding perturbations in the initial chirp. The pedestal energy generated in all three cases is only a fraction of a percent. The deviation in compression factor is small and is similar for all three cases. Thus the soliton is very robust to perturbations in the initial chirp in all three cases. We have carried out extensive numerical simulations on the perturbations of initial power and chirp by varying the decay rate of dispersion and changing the strength of quintic nonlinearity. In all cases we have studied, we find that the compressed pulse in the case of competing cubic-quintic nonlinearities has the smallest deviations in peak power and chirp. The pedestal energy is also the smallest, but the compression factor is also the smallest when compared to the case of pure cubic nonlinearity and cooperating cubic-quintic nonlinearities.

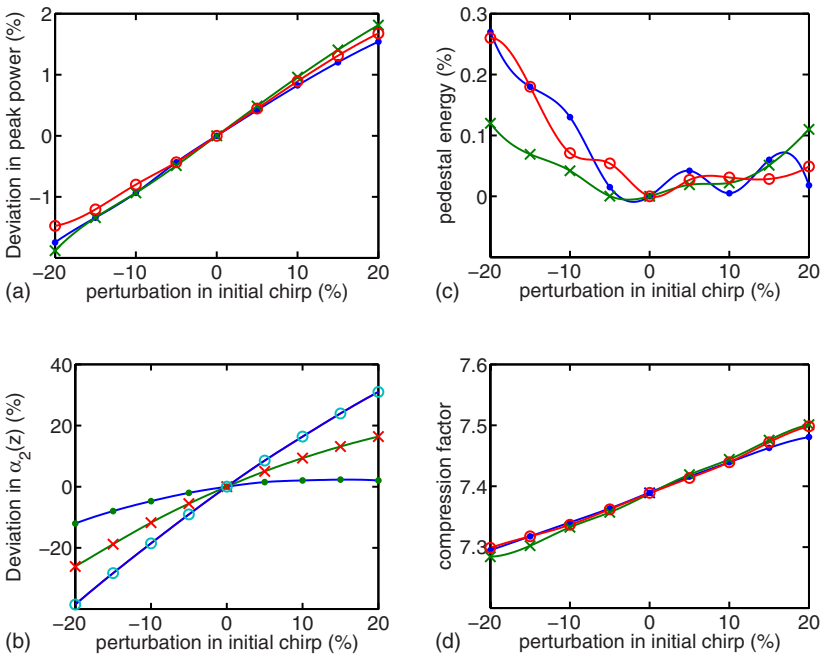

FIG. 4. (Color online) (a) Deviations of the peak power from the exact solution, (b) the chirp coefficient, (c) the pedestal energy, and (d) the compression factor at $L=400$ m when the initial chirp deviates from the chirp value of the exact solution from −20% to +20%. The physical parameters chosen are the same as those in Fig. 3. The dots represent results for competing cubic-quintic nonlinearities ($\delta_0=0.4724$ W^{-2} m^{-1}), circles represent the results for cooperating cubic-quintic nonlinearities ($\delta_0=-0.4724$ W^{-2} m^{-1}), and crosses represent the results for pure cubic nonlinearity ($\delta_0=0$).

Figure 5 shows the evolution of the (a) peak power from the exact values, (b) chirp, (c) pedestal energy, and (d) compression factor when the peak power of the initial solution is +20% larger than the ideal solution given in Eq. (21) for competing cubic-quintic nonlinearties and Eq. (22) for cooperating cubic-quintic nonlinearities. The distance traveled is 400 m. The parameter L_{D0} is the initial dispersion length as $z=0$. The dashed lines represent the soliton solution of the CQNLS equation. The dots represent perturbation results for competing cubic-quintic nonlinearties, the circles represent cooperating cubic-quintic nonlinearities, and the crosses represent pure cubic nonlinearity. From Figs. 5(a) and 5(d), the peak power and pulse width (and thereby compression factor) of the solitary pulse undergo periodic oscillations during the evolution. We note that the oscillation periods are different for the three different cases. Without quintic nonlinearity and for constant dispersion, the oscillation has a period of $8z_0$ for solitons where z_0 ($=\pi L_{D0}/2$) is the soliton period, because of the resonance of the perturbation with the soliton wave vector, $2\pi/(8z_0)$ [25]. Figures 5(b) and 5(c), respectively, represent the evolution of the chirp and pedestal energy generated.

In what follows, for the completeness of the investigation, we predict the oscillations exhibited by the peak power and pulse width during the evolution. Figure 6(a) represents the behavior of change in peak power $\Delta P=P_{\text{perturbed}}-P_{\text{ideal}}$ along the propagation direction when the initial input peak power deviates from the ideal peak power from −20% to +20%. We

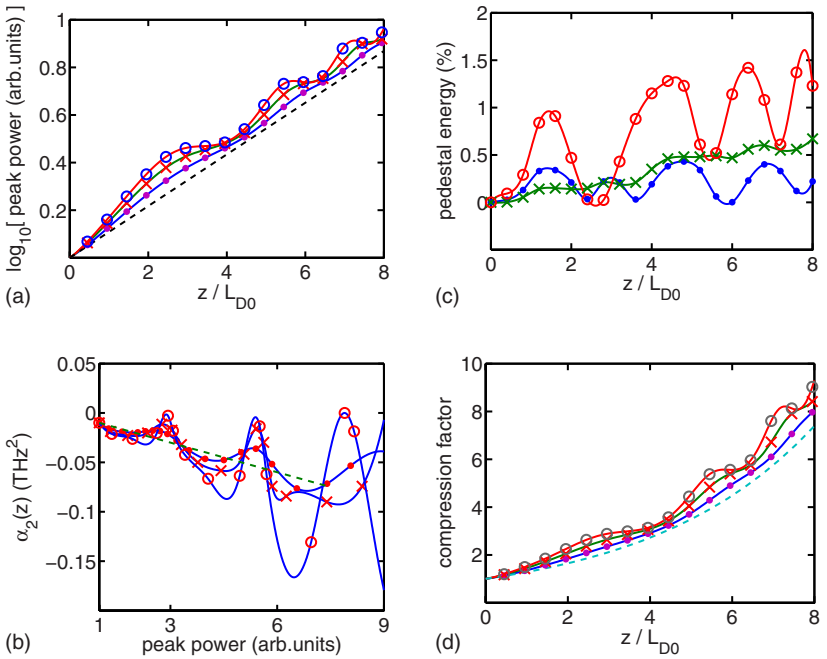

FIG. 5. (Color online) Evolution of the (a) peak power, (b) chirp, (c) pedestal energy, and (d) compression factor when the initial peak power deviates +20% from the ideal peak power when the distance varies from $z=0$ to 400 m for the same physical parameters used in Fig. 1. The parameter L_{D0} is the initial dispersion length. The dashed lines represent results for the exact solution, dots represent the competing cubic-quintic nonlinearities ($\delta_0=0.4724$ W^{-2} m^{-1}), circles represent the results for cooperating cubic-quintic nonlinearities ($\delta_0=-0.4724$ W^{-2} m^{-1}), and crosses represent the results for pure cubic nonlinearity ($\delta_0=0$).

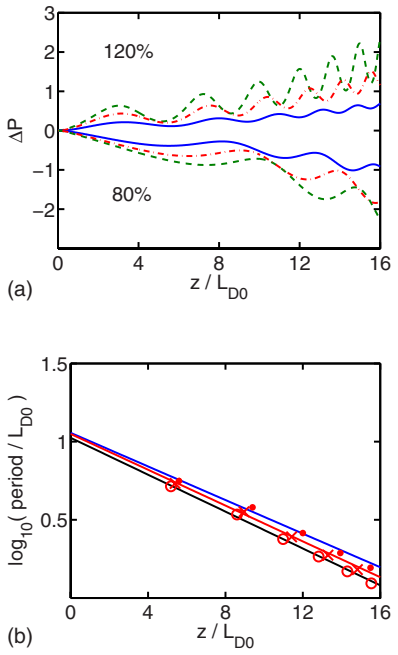

FIG. 6. (Color online) (a) Evolution of $\Delta P = P_{\text{perturbed}} - P_{\text{ideal}}$ along the propagation direction. The solid lines represent the results for competing cubic-quintic nonlinearities ($\delta_0 = 0.4724\ \text{W}^{-2}\ \text{m}^{-1}$), dashed lines represent the results for cooperating cubic-quintic nonlinearities ($\delta_0 = -0.4724\ \text{W}^{-2}\ \text{m}^{-1}$), and dot-dashed lines represent the results for pure cubic nonlinearity ($\delta_0 = 0$). The physical parameters are chosen as $\tau_0 = 5$ ps, $\beta_0 = -0.5\ \text{ps}^2\ \text{m}^{-1}$, $\sigma = 0.0025\ \text{m}^{-1}$, $\gamma_0 = 0.2362\ \text{W}^{-1}\ \text{m}^{-1}$, $\alpha_{20} = -0.005\ \text{THz}^2$, $g = 0$, and $z = 800$ m. (b) Variation of the oscillation periods along the propagation direction. The dots represent the results for competing cubic-quintic nonlinearities ($\delta_0 = 0.4724\ \text{W}^{-2}\ \text{m}^{-1}$), circles represent the results for cooperating cubic-quintic nonlinearities ($\delta_0 = -0.4724\ \text{W}^{-2}\ \text{m}^{-1}$), and crosses represent the results for pure cubic nonlinearity ($\delta_0 = 0$). The solid lines represent exponential fits for the three different cases.

have halved the dispersion decay rate and doubled the pulse propagation distance in Fig. 6(a) when compared to that used in Fig. 4 in order to observe more oscillation periods. The solid lines represent the competing cubic-quintic nonlinearities, dashed lines represent the cooperating cubic-quintic nonlinearities, and dot-dashed lines represent the pure cubic nonlinearity. From Fig. 6(a), the deviation ΔP is the smallest for the competing cubic-quintic nonlinearities case. Figure 6(b) shows that the period of oscillations decreases exponentially along the propagation direction. The solid lines represent exponential fits for the three different cases. The rate of change of the period is found to be $0.002\,474\ \text{m}^{-1}$ for the competing cubic-quintic nonlinearities (dots), $0.002\,716\ \text{m}^{-1}$ for the cooperating cubic-quintic nonlinearities (circles), and $0.002\,637\ \text{m}^{-1}$ for pure cubic nonlinearity (crosses). All three decay rates for the three different cases are close to the decay rate of the dispersion, which is $0.0025\ \text{m}^{-1}$. Thus, the period of oscillation decreases exponentially as the dispersion decreases along the propagation direction. The oscillations in ΔP represent a gradual adjustment towards ideal pulse shape

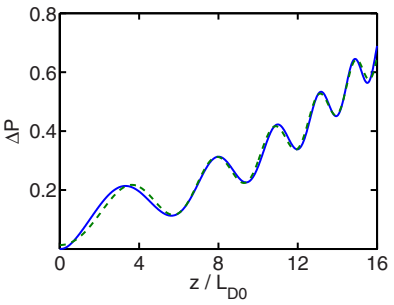

FIG. 7. (Color online) Curve fitting the evolution of ΔP for competing cubic and quintic nonlinearities by the function $f(\zeta) = c_1 \exp(c_2\zeta) + c_3 \exp(c_4\zeta)\sin[c_5 \exp(c_6\zeta)]$, where $\zeta = z/L_{D0}$ and c_i, $i = 1, \ldots, 6$, are constants. The solid line represents the simulation results of the evolution of ΔP for competing cubic-quintic nonlinearities when the initial peak power deviates +20% from the ideal value. The dashed lines represent the fitting results using the method of steepest descent where $c_1 = 0.0917$, $c_2 = 0.1238$, $c_3 = 0.08$, $c_4 = -0.0177$, $c_5 = -7.6532$, and $c_6 = 0.1043$, and the dashed lines represent the results for the fitting function.

under investigation. Figure 7 shows curve fitting of the evolution of ΔP for competing cubic-quintic nonlinearities with the function $f(\zeta) = c_1 \exp(c_2\zeta) + c_3 \exp(c_4\zeta)\sin[c_5 \exp(c_6\zeta)]$, where $\zeta = z/L_{D0}$ and c_i, $i = 1, \ldots, 6$, are constants. The solid lines represent the simulation results of the evolution of ΔP for competing cubic-quintic nonlinearities when the initial peak power is +20% larger than that of the ideal values. The dashed lines represent the curve-fitting results using the method of steepest descent where $c_1 = 0.0917$, $c_2 = 0.1238$, $c_3 = 0.08$, $c_4 = -0.0177$, $c_5 = -7.6532$, and $c_6 = 0.1043$.

Figure 8 shows the evolution of the (a) peak power, (b) chirp, (c) pedestal energy, and (d) compression factor when the initial chirp is +20% larger than that of the ideal solution. The dashed lines represent the soliton solution of the CQNLS equation. The dots represent perturbation results for competing cubic-quintic nonlinearties, the circles represent those for cooperating cubic-quintic nonlinearities, and the crosses represent those for pure cubic nonlinearity. We observe that the peak power and the compression factor (pulse width) of the solitary pulse undergo only very small periodic oscillations. The deviations in peak power and compression factor are very small. The pedestal energy undergoes relatively larger periodic oscillations during the evolution, but the magnitude of the variation is smaller than that for the perturbation in the peak power.

IV. CHIRPED SELF-SIMILAR TOWNES SOLITON

From the previous section, the soliton solution in the normal dispersion regime of the CQNLS equation with exponentially varying dispersion is unstable. Further, in the absence of quintic nonlinearity, the combination of cubic nonlinearity and normal dispersion, exponentially varying or not, does not support soliton solutions. However, a pure quintic nonlinear medium does support the soliton solution known as Townes solitons, which were discovered for the two-dimensional NLS equation in nonlinear optics and de-

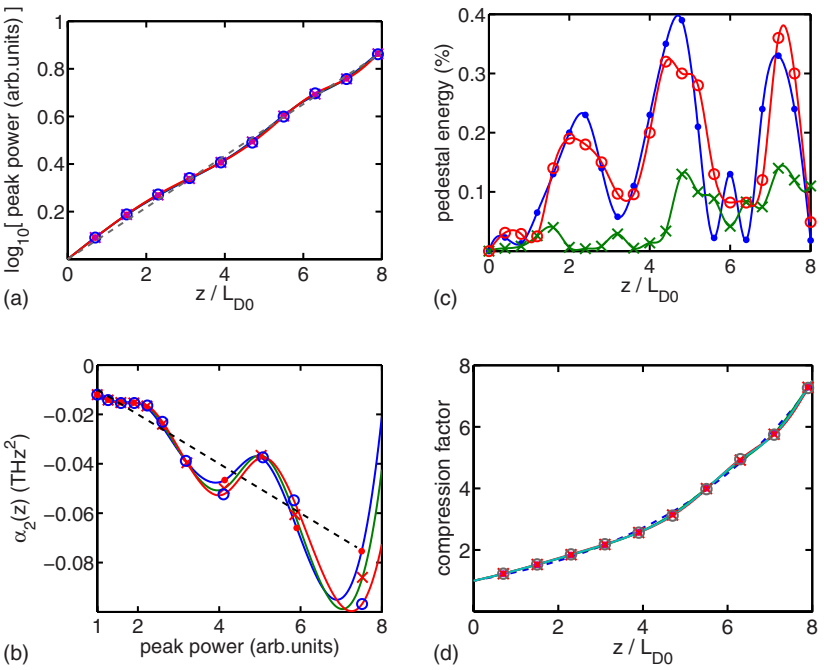

FIG. 8. (Color online) Evolution of the (a) peak power, (b) chirp, (c) pedestal energy, and (d) compression factor when the initial chirp deviates +20% from the exact chirp value when the distance varies from $z=0$ to 400 m for the same physical parameters used in Fig. 1. The dashed lines represent results for the exact solution, the dots represent the competing cubic-quintic nonlinearities ($\delta_0=0.4724$ W^{-2} m^{-1}), circles represent the results for cooperating cubic-quintic nonlinearities ($\delta_0=-0.4724$ W^{-2} m^{-1}), and crosses represent the results for pure cubic nonlinearity ($\delta_0=0$).

scribe the collapsing and dispersing of optical pulses [26]. Pulse propagation in a pure quintic NLS (QNLS) equation with distributed dispersion and distributed linear gain is given by

$$i\frac{\partial A}{\partial z}-\frac{\beta(z)}{2}\frac{\partial^2 A}{\partial \tau^2}-\delta(z)|A|^4A-i\frac{g(z)}{2}A=0. \tag{27}$$

Equation (27) describes nonlinear pulse propagation in many fields of nonlinear science—for example, in nonlinear optics under power-law nonlinearity. It is known that physically, various materials, including semiconductors, exhibit power-law nonlinearity. Spatial solitons have been investigated in media that have a power-law dependence on the intensity I^q for continuum values of q (with I being the intensity) [27]. However, in general, it may be difficult to find suitable nonlinear optical media which exhibit pure quintic nonlinearity because manipulation of the magnitude and the sign of nonlinearity is not easy. However, the QNLS equation aptly models BECs especially in the TG regime. Experimental generation of such a gas had also been reported [28]. Recently, it has been shown that the magnitude as well as the sign of nonlinearity, which are determined by the interactions between atoms in the condensate, could be manipulated by varying the external magnetic filed near the Feshbach resonance [29]. Therefore, it is physically relevant to discuss the chirped Townes soliton in BECs. The formation of solitons in BECs is similar to nonlinear optics, where the bright and dark solitons are supported by focusing and defocusing nonlinearities, respectively, whereas in BECs, the s-wave scattering interaction between atoms actually determines the soliton formation. Thus, bright and dark solitons are found in condensates with attractive and repulsive interactions. We now discuss the chirped Townes soliton in pure quintic media. The complex envelope of the chirped Townes soliton is obtained by applying the following physical condition $\beta(z)<0$ and $\delta(z)<0$ in Eq. (27):

$$A(z,\tau)=\frac{1}{\tau_0[1-\alpha_{20}D(z)]}\times\left[\frac{|\beta(z)|}{\sqrt{2\delta(0)\beta(0)/3}\,\tau_0^2}\,\mathrm{sech}\,2\left(\frac{\tau-\tau_c}{\tau_0[1-\alpha_{20}D(z)]}\right)\right]^{1/2}\times\exp(i\Phi). \tag{28}$$

The relation between the dispersion and the quintic nonlinear lengths is $2L_D/3=L_{n4}$. The energy and peak intensity of the chirped Townes soliton are given by

$$W=\frac{\sqrt{3}\pi|\beta(z)|}{[1-\alpha_{20}D(z)]\sqrt{8\delta(0)\beta(0)}},$$

$$A_{\max}^2=\frac{\sqrt{3}|\beta(z)|}{\tau_0[1-\alpha_{20}D(z)]^2\sqrt{2\delta(0)\beta(0)}}. \tag{29}$$

We then proceed to investigate the stability of the chirped Townes soliton. For the constant-coefficient case, it has been demonstrated that the Townes soliton is marginally stable in homogeneous media ($g=0$) according to the VK criterion. As has been discussed in Sec. III B, the VK criterion does not apply to the chirped Townes soliton in Eq. (28). However, unlike Sec. III B it is not possible to numerically establish that a solution is marginally stable. We would try to infer the character of the solution in Eq. (28) by numerically studying the evolution of inputs with amplitude above and below that of the solution. First we study the evolution of the analytic chirped Townes soliton. Figure 9 plots the evolution of analytic chirped Townes soliton solutions for constant (solid lines, $\beta_0=-0.5$ ps^2 m^{-1}), exponentially increasing (dot-dashed lines, $\sigma=-0.005$ m^{-1}), and exponentially decreasing (dashed lines, $\sigma=0.005$ m^{-1}) dispersions. The dots represent the results obtained by dint numerical simulations. Note that

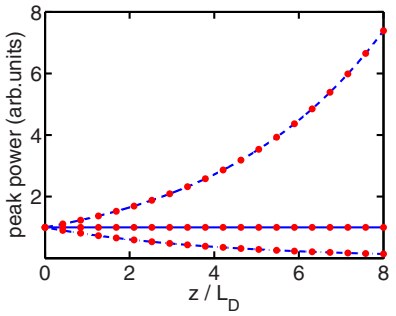

FIG. 9. (Color online) Evolution of the peak power of Townes solitons when the dispersion is constant (solid lines, $\beta_0=-0.5$ ps^2 m^{-1}), exponentially increasing (dot-dashed lines, $\sigma=-0.005$ m^{-1}), and exponentially decreasing (dashed lines $\sigma=0.005$ m^{-1}). The dots represent the results obtained by dint numerical simulation. The physical parameters are the same as those used in Fig. 1 except γ_0 (=0).

the analytical results are in good agreement with the results obtained by dint numerical simulations for the distance simulated.

So far, we have discussed the conventional pulse compression technique whereby we utilized the cubic nonlinearity and dispersion to achieve pulse compression. A nonconventional pulse compression technique based on the wave collapse phenomenon has also been reported [33]. It is well established that the pure quintic model exhibits collapse [30]. However, the occurrence of collapse could either be arrested or postponed by physical effects like damping, nonlinear saturation, etc. [31,32]. Recently, it has been shown that the quintic damping effect, which arises from the three-body interaction of an imaginary component, and cubic nonlinearity management help to arrest and/or suppress the occurrence of collapse [31].

Figure 10 shows the deviations of peak power from the exact Townes soliton when the input peak power deviates from the ideal peak power by (a) −5% and (b) +5% for constant dispersion (solid lines), exponentially decreasing dispersion (dashed lines), and exponentially increasing dispersion (dot-dashed lines). The physical parameters used are the same as those in Fig. 9. For constant dispersion (solid lines), the pulse disperses because the input power is less than the critical power, as shown in Fig. 10(a). When the dispersion increases exponentially (dot-dashed lines), the self-similar effect and the wave collapse act together to broaden the pulse. Thus the pulse undergoes fast broadening. When the dispersion decreases exponentially (dashed lines), the self-similar effect and the collapse act oppositely. Thus the pulse initially compresses slightly as the self-similar effect dominates, but eventually the wave collapse effect takes over and the pulse begins to broaden. The self-similar compression in the exponentially decreasing dispersion can be used to postpone the wave dispersion in a pure quintic medium.

Similarly, when the dispersion is constant, the pulse undergoes collapse when the input peak power is higher than the critical power, as shown by the solid lines of Fig. 10(b). Rapid compression can be achieved by the combined action of the collapse phenomenon and self-similar pulse compression in the exponentially decreasing dispersion (dashed lines). The occurrence of collapse is postponed in the case of exponentially increasing dispersion (dot-dashed lines) since the self-similar effect in the exponentially increasing dispersion acts against the collapse. Our numerical results show that the chirped Townes soliton exhibits a similar property as the Townes soliton with constant dispersion when the input peak power deviates from the ideal peak power. Thus it is likely that the chirped Townes soliton is also marginally stable.

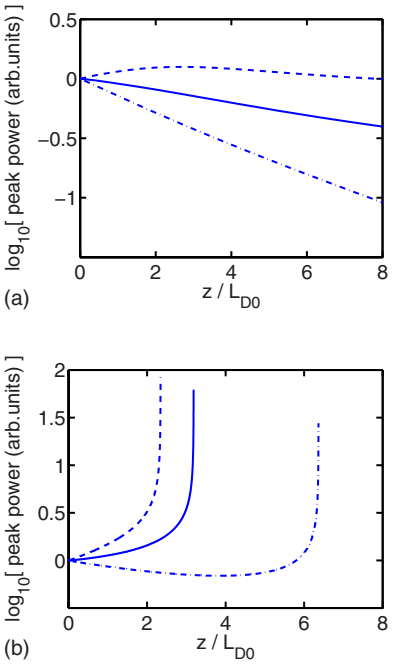

FIG. 10. (Color online) The deviations of peak power from the exact Townes soliton solution when the input peak power deviates from the ideal peak power by (a) −5% and (b) +5% when the dispersion is constant (solid lines), exponentially decreasing (dashed lines), and exponentially increasing (dot-dashed lines). The physical parameters are the same as those used in Fig. 9.

Finally, in general, it is difficult to realize a medium that exhibits pure quintic nonlinearity. It is therefore important to determine the tolerance of the chirped Townes soliton of a quintic medium in the presence of a small amount of cubic nonlinearity. Figure 11 shows the change in peak power of the Townes soliton in the presence of cubic nonlinearity. The dots represent the results of pure quintic nonlinearity. The solid line, dot-dashed line, and dashed line represent the results when the ratio of cubic nonlinear length to quintic nonlinear length (L_{n_2}/L_{n_4}) is 12 000, 1 200, and 120, respectively. Figure 11 shows that the evolution of the chirped Townes soliton is very sensitive to the presence of even a small amount of cubic nonlinearity ($L_{n_4}/L_{n_2}<0.1\%$). As the cubic nonlinearity increases, the chirped Townes soliton pulse becomes unstable. The three different values of cubic nonlinearity are $\gamma_0=10^{-5}$, 10^{-4}, and 10^{-3} W^{-1} m^{-1}. The other physical parameters are same as those in Fig. 1.

V. CONCLUSION

By using self-similar scaling analysis, we have found the chirped bright soliton solutions in the anomalous and normal

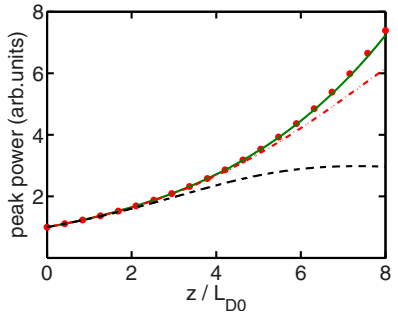

FIG. 11. (Color online) Evolution of the peak powers of chirped Townes solitons in the presence of cubic nonlinearity. The dots represent the results of pure quintic nonlinearity. The solid line, dot-dashed lines, and dashed lines represent the results when the ratio of cubic nonlinear length to quintic nonlinear length (L_{n_2}/L_{n_4}) is 12 000, 1200, and 120, respectively. The corresponding values of cubic nonlinearity are $\gamma_0=10^{-5}$, 10^{-4}, and 10^{-3} W^{-1} m^{-1}, respectively. The other physical parameters are same as those in Fig. 1.

dispersion regimes of cubic-quintic nonlinear media. By means of direct numerical simulations, we show that the chirped soliton in the anomalous dispersion regime is stable, whereas that in the normal dispersion regime is unstable. For these chirped solitons, the dispersion length, the cubic nonlinear length, and the quintic nonlinear length are related. If the quintic nonlinear length goes to infinity, the dispersion length will equal the cubic nonlinear length. We observed that by the use of exponentially decreasing dispersion, it is possible to utilize these self-similar solitons to achieve pedestal-free pulse compression in cubic-quintic nonlinear media.

We then studied the evolution of the chirped bright solitons when the initial peak power or the initial chirp is perturbed. We have found that the evolution of the soliton is not significantly affected even when the pertubation in the initial parameters is $\pm 20\%$ of its ideal values. The solitons have better tolerance to perturbations in the initial chirp than initial peak power. We have carried out extensive numerical simulations by varying the decay rate of dispersion and changing the strength of the quintic nonlinearity. From the numerical simulations, we have observed that competition between the cubic and quintic nonlinearities stabilizes the pulse against perturbations in initial pulse parameters. Hence, one can construct a stable pedestal-free optical pulse compressor by using competing cubic-quintic nonlinearities.

Finally, we studied the chirped Townes soliton in pure quintic nonlinear media. As the Townes solitons with constant dispersion are marginally stable, we studied the perturbation of the chirped Townes soliton in terms of peak power. We found that we can achieve fast pulse compression by combining the wave collapse and exponentially decreasing dispersion when the perturbation is higher than the ideal one. The occurrence of collapse can also be postponed by using exponentially increasing dispersive media. These two issues (fast and slow compression) could be implemented depending on the physical situation and requirement. Applications in terms of BECs in the TG regime have also been discussed.

ACKNOWLEDGMENTS

The authors acknowledge the support of the Research Grant Council of the Hong Kong Special Administrative Region, China (Project No. PolyU5289/07E). K.N. appreciates the hospitality of the Department of Electronic and Information Engineering at The Hong Kong Polytechnic University. K.N. also wishes to thank the Royal Society for support in the form of an International Joint Project Grant.

[1] G. P. Agrawal, *Nonlinear Fiber Optics* (Academic Press, San Diego, 2001).
[2] L. F. Mollenauer and J. P. Gordon, *Solitons in Optical Fibers: Fundamentals and Applications* (Academic Press, San Diego, 2006).
[3] G. P. Agrawal, *Applications of Nonlinear Fiber Optics* (Academic Press, San Diego, 2001).
[4] R. H. Stolen, J. Botineau, and A. Ashkin, Opt. Lett. **7**, 512 (1982); B. Nikolaus, D. Grischkowsky, and A. C. Balant, *ibid.* **8**, 189 (1983); R. Yatsu, K. Taira, and M. Tsuchiya, *ibid.* **24**, 1172 (1999); K. R. Tamura and M. Nakazawa, IEEE Photonics Technol. Lett. **11**, 230 (1999); M. D. Pelusi, Y. Matsui, and A. Suzuki, IEEE J. Quantum Electron. **35**, 867 (1999); K. R. Tamura and M. Nakazawa, IEEE Photonics Technol. Lett. **13**, 526 (2001); P. K. A. Wai and Wen-hua Cao, J. Opt. Soc. Am. B **20**, 1346 (2003).
[5] A. Mysyrowicz, A. Couairon, and U. Keller, New J. Phys. **10**, 025023 (2008); L. Berge, S. Skupin, R. Nuter, J. Kasparian, and J. P. Wolf, Rep. Prog. Phys. **70**, 1633 (2007); M. Nurhuda, A. Suda, and K. Midorikawa, J. Opt. Soc. Am. B **23**, 1946 (2006); A. Couairon, Phys. Rev. A **68**, 015801 (2003).
[6] A. Braun *et al.*, Opt. Lett. **20**, 73 (1995).
[7] S. Tzortzakis, L. Sudrie, M. Franco, B. Prade, A. Mysyrowicz, A. Couairon, and L. Berge, Phys. Rev. Lett. **87**, 213902 (2001).
[8] A. Dubietis, G. Tamosauskas, I. Diomin, and A. Varanavicius, Opt. Lett. **28**, 269 (2003).
[9] J. D. Moores, Opt. Lett. **21**, 555 (1996).
[10] M. E. Fermann, V. I. Kruglov, B. C. Thomsen, J. M. Dudley, and J. D. Harvey, Phys. Rev. Lett. **84**, 6010 (2000).
[11] V. I. Kruglov, A. C. Peacock, and J. D. Harvey, Phys. Rev. Lett. **90**, 113902 (2003); V. I. Kruglov, A. C. Peacock, and J. D. Harvey, Phys. Rev. E **71**, 056619 (2005).
[12] K. Senthilnathan, P. K. A. Wai, and K. Nakkeeran, in *Optical Fiber Communications Conference, Anaheim*, Report No. JWA19, 2007 (unpublished).
[13] K. Senthilnathan, K. Nakkeeran, K. W. Chow (unpublished).
[14] Y. S. Kivshar and G. P. Agrawal, *Optical Solitons: From fibers to photonic crystals* (Academic Press, San Diego, 2003).
[15] N. N. Akhmediev and A. Ankiewicz, *Solitons: Nonlinear pulses and beams* (Chapman and Hall, London, 1997).
[16] D. Mihalache, D. Mazilu, I. Towers, B. A. Malomed, and F. Lederer, Phys. Rev. E **67**, 056608 (2003).
[17] I. Towers, A. V. Buryak, R. A. Sammut, B. A. Malomed, L.-C.

Crasovan, and D. Mihalache, Phys. Lett. A **288**, 292 (2001).
[18] B. A. Malomed, L. C. Crasovan, and D. Mihalache, Physica D **161**, 187 (2002).
[19] D. Mihalache, D. Mazilu, L. C. Crasovan, I. Towers, A. V. Buryak, B. A. Malomed, L. Torner, J. P. Torres, and F. Lederer, Phys. Rev. Lett. **88**, 073902 (2002).
[20] J. Herrmann, Opt. Commun. **87**, 161 (1992).
[21] D. I. Pushkarov and S. Tanev, Opt. Commun. **124**, 354 (1996); S. Tanev and D. I. Pushkarov, *ibid.* **141**, 322 (1997).
[22] R. Hao, L. Li, Z. Li, R. Yang, and G. Zhou, Opt. Commun. **245**, 383 (2005).
[23] F. Smektala, C. Quemard, V. Couderc, and A. Barthélémy, J. Non-Cryst. Solids **274**, 232 (2000); C. Zhan, D. Zhang, D. Zhu, D. Wang, Y. Li, D. Li, Z. Lu, L. Zhao, and Y. Nie, J. Opt. Soc. Am. B **19**, 369 (2002); G. Boudebs, S. Cherukulappurath, H. Leblond, J. Troles, F. Smektala, and F. Sanchez, Opt. Commun. **219**, 427 (2003); K. Ogusu, J. Yamasaki, S. Maeda, M. Kitao, and M. Minakata, Opt. Lett. **29**, 265 (2004); F. Sanchez, G. Boudebs, S. Cherukulappurath, H. Leblond, J. Troles, and F. Smektala, J. Nonlinear Opt. Phys. Mater. **13**, 7 (2004).
[24] K. Senthilnathan, Qian Li, P. K. A. Wai, and K. Nakkeeran *Proceedings of PIERS Conference* (The Electromagnetic Academy, Cambridge, MA, 2007), Vol. 3, p. 531.
[25] J. P. Gordon, J. Opt. Soc. Am. B **9**, 91 (1992).
[26] R. Y. Chiao, E. Garmire, and J. C. H. Townes, Phys. Rev. Lett. **13**, 479 (1964).
[27] A. W. Snyder and D. J. Mitchell, Opt. Lett. **18**, 101 (1993); J. G. Ma, Microwave Opt. Technol. Lett. **19**, 54 (1998); S. Gangopadhyay and S. N. Sarkar, Fiber Integr. Opt. **20**, 191 (2001).
[28] B. Paredes, A. Videra, V. Murg, O. Mandel, S. Frölling, I. Cirac, G. V. Shlyapnikov, T. W. Wänsch, and I. Bloch, Nature (London) **249**, 277 (2004).
[29] S. L. Cornish, N. R. Claussen, J. L. Roberts, E. A. Cornell, and C. E. Wieman, Phys. Rev. Lett. **85**, 1795 (2000).
[30] C. Sulem and C. Sulem, *The Nonlinear Schrödinger Equation: Self-Focusing and Wave Collapse* (Springer, Berlin, 2000).
[31] Yu. B. Gaididei, J. Schjodt-Eriksen, and P. L. Christiansen, Phys. Rev. E **60**, 4877 (1999); F. Kh. Abdullaev and J. Garnier, Phys. Rev. A **70**, 053604 (2004); Phys. Rev. E **72**, 035603(R) (2005); F. Kh. Abdullaev and M. Salerno, Phys. Rev. A **72**, 033617 (2005).
[32] G. L. Alfimov, V. V. Konotop, and P. Pacciani, Phys. Rev. A **75**, 023624 (2007).
[33] Sergei K. Turitsyn, Phys. Rev. A **47**, R27 (1993).